Eur. Phys. J. B **42**, 373–380 (2004)
DOI: 10.1140/epjb/e2004-00393-4

THE EUROPEAN PHYSICAL JOURNAL B

Diffraction study of the piezoelectric properties of low quartz

R. Guillot[1], P. Fertey[1,a], N.K. Hansen[1], P. Allé[1], E. Elkaïm[2], and C. Lecomte[1]

[1] Laboratoire de Cristallographie et Modélisation des Matériaux Minéraux et Biologiques, UMR-CNRS-7036, Université Henri Poincaré – Nancy I, BP 239, 54 506 Vandoeuvre-lès-Nancy Cedex, France
[2] LURE, Centre Universitaire Paris-Sud, Bât. 209D, BP 34, 91898 Orsay Cedex, France

Received 22 September 2004
Published online 23 December 2004 –

Abstract. The effect of a static electric field on the crystal structure of α-quartz has been determined by Xray diffraction on single crystals. By a stroboscopic technique rocking curves are measured quasi simultaneously for zero field and for two opposite strong fields (28.8 kV/cm) applied in the direction of the crystallographic a-axis. The relative intensity-changes of high order reflections (i.e. sensitive to the core electrons) were measured and analysed by a least squares method technique. The analysis indicates that the bond distances Si-O are very little affected by the field, but both a deformation and a reorientation of the SiO_4 tetrahedra are induced. The model is qualitatively in agreement with the small amplitudes of the induced polarisation and the piezoelectric coefficients.

PACS. 61.10.Nz X-ray diffraction – 77.65.-j Piezoelectricity and electromechanical effects – 77.22.Ej Polarization and depolarization – 07.85.Qe Synchrotron radiation instrumentation

1 Introduction

α–quartz is the most widely used piezoelectric material at present. The structure of α-quartz is formed of corner-sharing SiO_4 tetrahedra and crystallizes in the trigonal $P3_121$ or $P3_221$ space groups (left-handed and right-handed respectively). Structure-property relationships have been developed for α-quartz and its homeotypes MXO_4 (M = B, Al, Ga, Fe; X = P, As) relating many physical, thermodynamic, dielectric and piezoelectric properties of these materials to the amplitude of structural distortions.

The homeotype structure corresponds to a cation-ordered derivative of the α-quartz type with a doubled c parameter. In particular, the piezoelectric coupling coefficient was found to increase linearly as a function of the tetrahedral tilt angle which is the order parameter of the $\alpha \rightarrow \beta$ phase transition (at 573 °C for quartz) and the intertetrahedral Si-O-Si bridging angle [1]. The temperature and pressure behaviors can also be understood in a unified way considering these structural distortions [2]. However, the origin of the piezoelectric properties and the polarization is not clear. The direct investigation at the atomic level of the structural distortions induced by an applied electric field should help to clarify the relevance of the structural contributions.

In most text books, the origin of the polarisation of quartz resulting from the piezo electric effect is described by pure ionic displacements of the Si^{4+} and O^{2-} ionic sublattices (i.e. the *Meissner model*) [3]. However, Si-O bonds are known to be only partially ionic [4].

Going beyond the ionic model, Pietsch et al. have suggested that the main effect of an external electric field, applied along the a axis of α-quartz, is a change of the bonding angle between oxygen and silicon (i.e. bridge angle) [5]. Recently Davaasambuu et al. described the inverse piezo electric effect by the rotation of connected rigid SiO_4 tetrahedra [6,7]. Both models result from an X-ray diffraction approach. A few Bragg reflections were measured using a field switching technique ($hh0$ and $h00$). Due to missing information perpendicular to the field direction, these authors assumed volume conservation of the SiO_4 tetrahedra under the influence of the external electric field, i.e. the SiO_4 tetrahedra were rotated as rigid objects against each other. As a consequence, the displacements of the atoms were constrained and the atoms could not move freely [6]. Furthermore, they report very small variations of bond angles (about few hundredth of a degree) that hardly exceeds the experimental errors.

It is also to be noted that in a review of the structure to dielectric, elastic and chiral properties relationships in crystals, Abrahams has already underlined that for the direct piezoelectric effect, rotations of rigid tetrahedra under tensile stress would not explain the order of magnitude of the observed piezoelectric moduli [8]. In order to understand the influence of an external electric field on the structural properties of α-quartz with no a priori, we have performed X-ray diffraction measurements on X cut plate samples to which an external, periodically reversed

[a] e-mail: pierre.fertey@lcm3b.uhp-nancy.fr

electric field (electric field parallel to the [100] direction) is applied. The next paragraphs describe the experimental method and present our first results. The amplitudes of the induced polarization and the piezoelectric coefficients are then discussed based on our structural model.

2 Experimental technique and methods of data analysis

2.1 Experimental technique

From high resolution X-ray diffraction data it is possible to obtain the atomic structure and electron density distribution with a high accuracy. Unfortunately, this information only concerns the ground state or the non perturbed structure of the crystal. A similar experiment, performed with a crystal onto which an external electric field is applied, will give a relevant information on the induced effects. However, applying a static field to a sample will, in most cases, induce irreversible effects such as charge accumulation, ionic conduction or defect migrations, which may mask the properties to be studied.

Puget and Godefroy were the first to propose a field-switching method: the field direction is periodically reversed at a low frequency in order to remedy the mentioned drawbacks [9]. We have developed our own instrument for performing this kind of experiments [10]. Diffraction profiles are measured by a step-by-step technique where an in-situ electric field is simultaneously applied to the crystal. This field is generated by a high voltage V directly applied to the extended faces of the crystal. The direction of the field is periodically reversed and the diffracted photons are counted in separate channels, synchronized with the particular field direction. In this so called field-switching method, the rocking curves of the excited ($V = V_+, V_-$) and ground states ($V = 0$) are thus measured quasi simultaneously.

When an electric field is applied to a piezo electric crystal, the diffraction is affected in two ways: the Bragg angles (θ_B) are changed ($\Delta\theta_B \sim 0.001 - 0.01°$) via the converse piezo electric effect and so are the Bragg intensities (few % relative variations).

The Bragg angle change can be predicted from the known piezo electric constants, and this is a powerfull check on the actual electric field strength and homogeneity in the sample. This has already been discussed by Bhalla [11] and Barsch [12]. On the other hand, the piezoelectric tensor can be determined if several Bragg angle shifts are measured.

Small variations of the diffracted intensities may be induced by i) crystal symmetry changes: these can be detected by a careful analysis of the intensity distribution in the reciprocal space (e.g.: extinction rules and symmetry relations between reflection intensities) ii) atomic displacements and electron density polarisation and iii) crystal perfection: the Bragg intensity is very sensitive to crystal perfection (primary or secondary extinction). It will therefore be very sensitive to possible field induced alterations. These may lead to much larger intensity changes than expected from structural modifications.

Therefore, the determination of structural variations/distortions induced by the applied electric field relies on the ability to distinguish between these phenomena.

2.2 Samples

The quartz crystal used in the present study has been grown by the Société Industrielle de Combustible Nucléaire (Annecy, France). From the crystal habit it was deduced that this crystal was a right-handed α-quartz (spacegroup is $P3_221$). Plate like samples with typical dimensions of $5 \times 5 \times 0.52$ mm^3 were cut from this master crystal with their extended faces parallel to the $(2\ {-1}\ 0)$ Miller plane (X cut). The faces were polished and 3×3 mm^2 aluminium electrodes were vapour deposited. The sample was glued on an insulating sample holder and the high voltage contact was realised using silver varnish.

Preliminary measurements to check possible "quality" variation induced by the applied electric field were performed using the topography beam line D25 at LURE. No significative profile variations were observed on the 2-10 and 020 rocking curves, neither as a function of the electric field nor as a function of time. It was deduced that the electric field applied has no influence on the intrinsic crystalline quality.

Using the field switching technique, rocking curve measurements with scattering vectors larger than 0.7 Å^{-1} were performed. With this choice, the scattered intensity comes predominantly from the core electrons of each atom and the scattering coming from the valence electrons (involved in chemical bonding) is negligible leading to a high accuracy on the relative positions of the atoms. 25 Bragg reflections were measured at the DW22 synchrotron beamline at LURE. The data were complemented by 11 strong lines measured with our instrument connected to our laboratory diffractometer (sealed-tube, Nonius CAD4). Table 1 recapitulates the experimental conditions.

2.3 Refinement

Due to the limited number of scattering measurements, it was advantageous to perform the structural analysis of the influence of the field in terms of departure from an unperturbed structure. We have modified the structure and electron density refinement program MOLLY [13] to perform this task. The structural modifications (Δp_i) of a parameter p_i are determined by means of a least squares method refinement using, as inputs, the relative intensity variations $\eta_{+(-)} = (I_{+(-)} - I_0)/I_0$ rather than the scattering intensity $I_{+(-)}$ itself. Here $I_{+(-)}$ and I_0 denote the scattering intensities for the $+(-)E$ (perturbed crystal) and $E = 0$ (unperturbed crystal) fields respectively. Due to the special technique used to measured the Bragg scattering intensities [10], a unit weighting scheme was adopted in the least squares refinements. Furthermore, the refined parameters p_i were limited to atomic coordinates only.

Table 1. Experimental conditions. r_{eq} is the equivalent ratio of the number of reflections to the number of refined parameters (the introduction of restraints is equivalent to increasing the number of observations).

Crystal data		
Chemical formula	SiO_2	
Temperature	293 K	
Cell setting	Hexagonal	
Space group	P 3_221	
a (Å)	4.910(1)	
c (Å)	5.401(1)	
V (Å^3)	112.76	
Data collection		
Diffractometer	Nonius CAD4	W4Diff
Radiation type	Sealed tube	Synchrotron
Wavelength (Å)	0.710	0.688
$(\sin\theta/\lambda)_{min}$ (Å^{-1})	0.7	0.7
No. of reflections	11	25
Scan mode	omega	omega
scan range	1° to 1.5°	0.05° to 0.1°
Electric field		
amplitude (kV/cm)	28.8	
switching frequency	25 Hz	
duration of each E value	10 ms	
delay after E switching	2.75 ms	
photon count at each E	7 ms	
No. of switchings/ω step	100	100
meas. time for 1 scan	4h	15'
Refinement		
Model[a]	no. of restraints	r_{eq}
free	0	2.3
restrained	6	2.8
rigid	16	3.7

[a] see text.

The structure model of α-quartz from Le Page was taken as the unperturbed structure [14].

3 Results and discussion

3.1 Piezoelectric displacements

Figure 1 presents the Bragg shifts of the $(2h\ -h\ 0)$ lattice planes for $h = 2$, 3, 4, 5 and 6. As expected, a linear behaviour is observed. When the electric field E is applied along the a cell axis, the Bragg shifts $\Delta\theta_B$ for these reflections are simply related to the d_{11} piezo electric coefficient by $\Delta\theta_B = E\ d_{11}\ \tan\theta_B$ where θ_B is the Bragg angle [12]. From the slope of a linear fit, the d_{11} was found to be 2.1 pC/N which is in excellent agreement with the known value 2.3 pC/N [15]. From the close agreement between these values, it was concluded that the electric field in the sample volume probed by the X-rays is homogeneous.

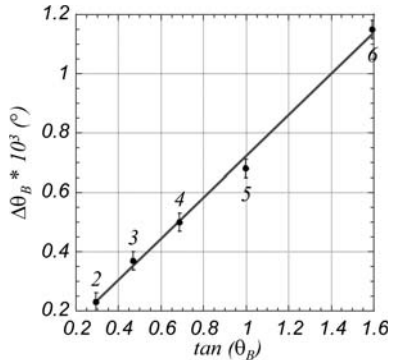

Fig. 1. Bragg angle shifts of the *(2h -h 0)* Bragg planes as a function of $\tan(\theta_B)$ for $h = 2$, 3, 4, 5 and 6.

Table 2. Comparison of measured intensity variations in this work and in [6].

$h\ k\ l$	η_+ this work	η_+ [6]
12 −6 0	0.16	−1.63
10 −5 0	−0.33	−0.23
8 −4 0	−0.40	−0.37

3.2 Induced intensity modulations

As expected, the field induced scattering intensity variations $\eta_{+(-)}$ are small (∼1% or less). The η_+ and η_- values for each profile have opposite signs and their absolute amplitude are in good agreement [16]. A maximum of $\eta_+ = 2.0\%$ was measured for the 840 reflection. Two Friedel pairs (anomalous dispersion of O and Si can be neglected) and three pairs of equivalent Bragg reflections, i.e. symmetrically equivalent by the two fold axis along the a direction, were present in the data set. The degree of consistency of their $\eta_{+(-)}$ was within the experimental error and assesses the reliability of the measurements.

The data set contains three reflections which have also been measured by Davaasambuu et al. [7]. In Table 2 we compare the results. It is noted that we do not agree on the magnitude of the $12-60$ reflection. We observe almost no variation whereas in [6] the authors have found a strong effect (∼1.6% at 30 kV/cm). The origin of this difference is not clear.

3.3 Atomic displacements

The electric field being applied parallel to one of the two-fold rotation axes, the deformed structure will have the space group symmetry $C2$. However, we keep describing the atomic positions in the primitive unit cell obtained directly from the original hexagonal cell as illustrated in Figure 2. This figure also displays the labels of the atoms.

In the perturbed structure there are two symmetrically independent silicon atoms, one on the two-fold rotation axis (labelled Si_1), the other being at a general position (labelled Si_2). The origin of the cell is fixed by the Si_1

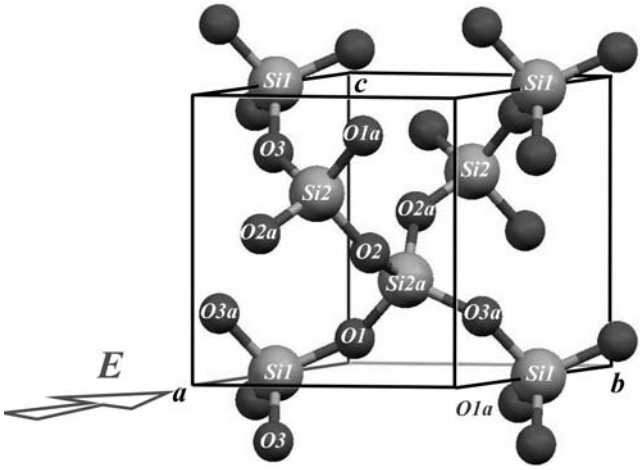

Fig. 2. Perspective view of the α-quartz structure.

position: its coordinates are therefore not refined. Among the six oxygen atoms in the unit cell, three are symmetrically independent in the deformed structure. A total of twelve parameters must therefore be refined to describe the atomic displacements under the influence of the electric field.

In a first refinement, no restraint was introduced (*free model*). The refinement converges satisfactorily but high correlation coefficients were obtained between atomic coordinates. Since Si-O bond distances were found to be hardly affected by the electric field, we have introduced weak restraints on the Si-O bond distances in order to decrease the correlations (*restrained distance model*). In order to test the rigid SiO_4 unit hypothesis of Davaasambuu et al. [7], a last refinement was performed where the Si-O and O-O distances were restrained (*rigid model*).

The reliability index minimized in this study is the weighted deviance sum which is defined in the following way:

$$\Sigma = \Sigma_i \left[w_i * (\mathrm{O}_i - \mathrm{C}_i)^2 \right],$$

where the sum is over the measured reflections, O_i and C_i are respectively the observed and calculated intensity variations, and w_i are kept constant ($2{\times}10^{-3}$). The values of Σ obtained are 52.2, 83.5 and 235.3 for the *free model*, the *restrained-distance model* and the *rigid model* respectively. It is clear that the differences between the *free model* and the *restrained distance model* are relatively small but we find that the correlation coefficients are largely decreased for the latter. On the contrary, the rigid SiO_4 model disagrees with our measurements: both rotations and deformations of the basic tetrahedral units are therefore requested to describe the field induced variations. From now on, only the refinement results of the restrained-distance model are discussed. The observed and calculated intensity variations are reported in Appendix A.

The field induced displacements of all the atoms are reported in Table 3. All the induced displacements are quite small (max relative variation of 1.3%). They cannot be explained by the volume change due to the converse piezoelectric effect which is about one order of magnitude smaller. The atomic displacements occur mainly in a plane perpendicular to the direction of the field. From Table 3, one can deduce that the Si_2 atoms are mainly displaced along the $\boldsymbol{c}$ direction when the field is applied. Since Si_2 tetrahedra form chains along the $\boldsymbol{a}$ direction (cf. Fig. 2), the field tends to bring these chains closer together. Furthermore, the field induces no variation of the centre of gravity of Si atoms and O atoms along the field direction; respectively $-0.0008(10)$ Å and $-0.0002(10)$ Å. As expected, this demonstrates the failure of the Meissner model: no relative rigid displacements of the Si and O occurs and cannot be at the origin of the polarization observed in the crystal.

The structural variations induced by the electric field are characterized by the internal deformations of the tetrahedra and the relative rotations of the corner linked SiO_4 groups.

In Table 4, angles in the perturbed and unperturbed structures are compared. Table 5 displays the overall rotation of each Si-O bond with respect to the axis of the

Table 3. Atomic displacements (in Angstroms) along the axes of the Cartesian framework ($x\|\boldsymbol{a}$, $y\|\boldsymbol{b^*}$ and $z\|\boldsymbol{c}$). Si_{2a} and O_{ia} atoms are the symmetry equivalents of the Si_1 and O_i atoms respectively by the two-fold rotation axis along the x direction.

Atom	Δx	Δy	Δz
Si_1	0	0	0
Si_2	−0.0001(4)	0.0005(6)	−0.0090(16)
O_1	−0.0006(17)	−0.0074(22)	0.0082(36)
O_2	0.0013(5)	0.0002(8)	−0.0065(24)
O_3	−0.0011(14)	−0.0049(24)	0.0032(32)

Table 4. Angles in the unperturbed and perturbed states (error = 0.08°), $\Delta = \alpha(E = 28$ kV/cm)-$\alpha(E = 0)$.

Angle α (°)	$E = 0$	$E = 28$ kV	Δ
O_1-Si_1-O_{1a}	109.07	108.94	−0.13
O_1-Si_1-O_3	110.41	110.62	0.21
O_1-Si_1-O_{3a}	108.68	108.40	−0.22
O_3-Si_1-O_{3a}	109.58	109.86	0.28
O_{2a}-Si_{2a}-O_{3a}	110.41	110.52	0.11
O_{2a}-Si_2-O_{3a}	108.68	109.22	0.54
O_{2a}-Si_{2a}-O_1	109.58	109.44	−0.14
O_{3a}-Si_1-O_{3a}	108.68	108.56	−0.12
O_{3a}-Si_2-O_{3a}	109.07	109.05	−0.02
O_1-Si_2-O_{3a}	110.41	110.06	−0.35
Si_1-O_{1a}-Si_2	143.67	143.82	0.15
Si_{2a}-O_{3a}-Si_1	143.67	144.05	0.38
Si_2-O_{2a}-Si_{2a}	143.66	143.26	−0.40
Si_2-O_2-Si_{2a}	143.66	143.26	−0.40
Si_1-O_1-Si_{2A}	143.67	143.82	0.15
Si_{2a}-O_{3a}-Si_1	143.67	144.05	0.38

Table 5. Overall rotations R_i of the Si-O bonds around the ith cartesian axis defined in the caption of Table 3 (error = 0.08°).

Bond	R_x	R_y	R_z
Si_1-O_1	0.47	0.32	0.20
Si_1-O_{1a}	0.47	−0.32	−0.20
Si_1-O_3	0.12	0.11	0.24
Si_1-O_{3a}	0.12	−0.11	−0.24
average	0.29	0	0
Si_{2a}-O_2	−0.51	0.53	−0.015
Si_{2a}-O_{2a}	0.03	−0.02	−0.016
Si_{2a}-O_{3a}	−0.30	−0.40	−0.01
Si_{2a}-O_1	−0.15	0.03	−0.05
average	−0.23	0.03	−0.02

Table 6. Angle between the Si-O bonds and the electric field direction (error = 0.08°), $\Delta = \alpha(E = 28\ \text{kV/cm}) - \alpha(E = 0)$.

Bond	$E = 0$	$E = 28$ kV	Δ
Si_1-O_1	54.53	54.46	−0.07
Si_1-O_{1a}	54.53	54.46	−0.07
Si_1-O_3	54.79	54.93	0.14
Si_1-O_{3a}	54.79	54.93	0.14
Si_{2a}-O_2	25.22	24.72	−0.50
Si_{2a}-O_{2a}	51.53	51.52	−0.01
Si_{2a}-O_{3a}	71.07	71.02	−0.05
Si_{2a}-O_1	92.62	92.60	−0.02

Cartesian frame work. In Table 6 the tilt of the Si-O bonds with respect the direction of the field is reported.

3.3.1 O-Si-O angle

As reported in Table 4, the two independent tetrahedra show different O-Si-O angle behaviour: the Si_2 (Si_{2a}) tetrahedra seem more affected than the Si_1 tetrahedron situated on the two fold axis, since all the angles show variations for the former, whereas only two angles are significantly changed for the latter. The significant increase of +0.5° of the O_{2a}-Si_{2a}-O_2 angle is consistent with a realignment of the Si_{2a}-O_2 bond parallel to the direction of the field (cf. Tab. 6). From Table 6, it can also be deduced that no other bond realignment is significant. For the Si_1 tetrahedron, the O-Si_1-O angle variations induced by the field have opposite trends which would be expected from the displacements of negatively charged oxygen atoms in the applied electric field: i.e. O_3-Si_1-O_3a increases while O_1-Si_1-O_1a decreases.

In order to get a better understanding of the field induced internal deformations of the two independent SiO_4 polyhedra, the continuous symmetry methodology can be applied [17,18]. The continuous symmetry measure (CSM) concept quantifies the departure of a nonsymmetric object from a desired G symmetry: e.g.: the departure or distortion of the SiO_4 units from perfect T_d symmetry. The symmetry measure $S(G)$ defines the minimal distance that the corners of a particular polyhedron have to be translated in order to attain the desired G symmetry. If the starting object has the G symmetry, then $S(G) = 0$, and S increases as it departs from the G symmetry (see [19] and references therein for details about CSM and the definition of S, applied in the case of α-quartz). Table 7 gives the symmetry measures of the non perturbed and perturbed structures.

Table 7. Symmetry measure of the SiO_4 and $SiSi_4$ units in α-quartz.

polyhedron	*S(Td)* $E = 0$ kV/cm	*S(Td)* $E = 28$ kV/cm
$(Si_1)O_4$	0.0083	0.0164
$(Si_2)O_4$	0.0083	0.0084
$(Si_1)Si_4$	4.6581	4.6588
$(Si_2)Si_4$	4.6585	4.6591

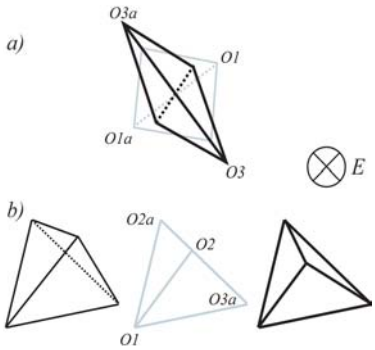

Fig. 3. Projection along the field direction of the schematic deformations of *a*) the SiO_4 unit on the two fold axis for $E = 0$ (light-grey) and $E = 28.8$ kV/cm (black), and *b*) of the Si_2 unit for $E = 0$ (left) and $E = 28.8$ kV/cm (right) compared to a perfect tetrahedron (middle).

In Table 7, the symmetry measure of the second nearest neighbours for the Si are also reported, i.e. distorted $SiSi_4$ tetrahedra. S takes *very small values* for the SiO_4 units but nevertheless significative, as pointed out by Yogev-Einot et al. [20]. The two independent SiO_4 tetrahedra behaves differently when the field is applied. The tetrahedricity of the Si_1 units is less pronounced as expected from the variations of the internal O-Si-O angles. Figure 3a schematically displays the decrease of tetrahedricity induced by the field.

On the contrary, the symmetry measure of the Si_2 tetrahedra seems not affected by the field. This is consistent with the internal O-Si-O angle variations if the minimal translations to be undergone by the O atoms to reach the T_d symmetry are accidentally equivalent in zero electric field or when a 30 kV/cm field is applied, as schematically represented in Figure 3b (remembering that $S(T_d)$ is always a positive number).

The $SiSi_4$ polyhedra are almost not affected by the field. This is different from the symmetry variations observed when the temperature or the pressure is varied: in those cases, the SiO_4 units are far less affected than $SiSi_4$ [20].

3.3.2 Bridging angle

The field induced effects on the bridging angle are of the same order of magnitude as the variations observed for the internal O-Si-O angles. A decrease of the bridge angle between the Si_2 units forming chains parallel to the direction of the field is $-0.40°$. This is consistent with the translation of the Si_2 chains toward one another along the z direction. As a consequence, the bridging angle between Si_1 and Si_2 units (in a plane almost perpendicular to the field direction) increases (average value 0.26°).

3.3.3 Overall rotation

The rotation of a tetrahedron may be defined as the average rotation of the four Si-O bonds about the three orthogonal axes of the Cartesian framework. Table 5 reports the individual Si-O bond rotations. Since the tetrahedra are slightly deformed by the field, no overall rotation are observed with respect to the y and z axis. The reorientation of the tetrahedra considered as more or less rigid entities, occurs mainly as a small rotations with respect to the direction of the field in clockwise-anticlockwise movements ($\pm 0.26°$ rotation).

These effects can be compared to the deformation induced by a hydrostatic pressure. It has been observed that the compression of the quartz structure is accomplished by primarily a tetrahedral tilting (i.e. rotations of the tetrahedra around their two-fold axis) and subsequently by an increased tetrahedral distortion [21,22]. It was demonstrated that the bridging angle variations are most effective to accommodate the pressure compression, but the O-Si-O variations are far from negligible: roughly speaking, the former are about three times greater than the latter depending on the pressure applied (respectively about 10% and 3% relative variations when the pressure is increased from ambient conditions to 10 kbar).

Similar effects are observed when an electric field is applied along the [100] direction: the overall rotation of the tetrahedra are mainly around the two fold axis and deformations of the tetrahedra are present. Differences exist since the amplitude of the variations in the bridging and O-Si-O angles are comparable, but this should be a consequence of a non hydrostatic perturbation of the structure.

Livien et al. [21] and Glinnemann et al. [22] have also demonstrated that the pressure induced variations of the volume of the SiO_4 units are hardly significant when compared to the O-Si-O or bridging angle variations. Therefore, the pressure behaviour and the results of this study contradict the rigid tetrahedral model which is generally accepted, in particular in [7].

In summary, one can therefore deduce that internal angular deformations are as important as bridging angle deformations to explain the field induced effects in α-quartz. These results contradict the model of Davaasambuu et al. [7] who have considered only the field induced variations of the bridging angle (along the field direction). Furthermore, we observe deformations which are about one order of magnitude larger.

4 Polarisation

Our structural model can qualitatively explain the small amplitude of the polarisation induced by the field. The tetrahedra are distorted even at zero external electric field in a such a way as to carry small pseudo dipole moments. It is therefore conceivable that, when applying an electric field, they will rotate. In zero field, because of the crystal symmetry, the contributions from the different tetrahedra to the overall dipole moment of the unit cell cancel. When the field is applied, deformation and reorientation of the tetrahedra are enhanced. In particular, the dipole component along the field direction is increased by rotations of the Si-O bonds around the y and z axis (cf. Tab. 5). Furthermore, the symmetry properties are lowered since only a two-fold axis along the field direction is conserved. Therefore the sum of the individual dipole moments does not vanish but remains small. This model is then qualitatively consistent with the small value of the d_{11} piezo electric coefficient and agrees with Abrahams' conclusions [8].

In this work, charge transfers between atoms and bond polarization have not been studied. However our structural model is consistent if one considers the overall displacements of the electron density within the bonds induced by an electric field applied along the [100] direction. For example, the O_1 atom would become less negative while the valence bond density should shift towards the O_3 atom. The internal O-Si-O angle variations observed in this study are therefore consistent with the rough effect of electrostatic repulsions. Analogous qualitative conclusions can be given for the Si_2 unit. Experimental investigations have been undertaken to measure polarization effects of the covalent Si-O bonds in α-quartz.

The X-ray diffraction analysis does not really explain the piezo electric effect. The *external* (macroscopic) *strain* manifests itself by small changes in Bragg angles because of modifications in the unit cell parameters. The *internal strain*, which should rather be termed polarisation, is basically a dielectric phenomenon, the result being variations in Bragg intensities. The internal and external strains are obviously connected, however, in our analysis of the intensity variations, the unit cell parameters are necessarily imposed, and the structural modifications, which we find, will in consequence satisfy the piezo electric behaviour. For explaining it, we do not see any other possibility than using a more theoretical approach. A possibility would be using band structure type calculations with a Berry's phase formalism in order to describe properly induced polarisations and overall strain. Experimental studies of how structure and possibly electron density is affected by external fields will in this context serve as a verification of certain aspects of the theory.

5 Conclusions

The structural variations induced by an applied electric field on the $\alpha-$quartz structure has been investigated by X-ray diffraction. The number of structure factors measured has allowed to propose a structural model with no

Table 8. Observed and calculated field induced intensity relative variations for the free (η_+^{free}), restrained (η_+^{rest}) and rigid (η_+^{rigid}) models. L and C label the reflections measured at LURE and with a CAD4 respectively.

	H	K	L	F^2	η_+^{obs} (%)	η_+^{free} (%)	η_+^{rest} (%)	η_+^{rigid} (%)
C	−10	5	0	57.13	0.17	0.15	0.13	0.08
C	10	−5	0	57.09	0.18	0.15	0.13	0.08
L	10	−5	0	57.09	0.18	0.15	0.13	0.08
L	8	−4	−2	37.04	−0.91	−0.88	−0.83	−0.79
L	8	−4	2	37.04	−0.74	−0.88	−0.83	−0.79
C	8	−4	−2	37.11	−0.86	−0.88	−0.84	−0.79
C	−8	4	2	37.42	−0.80	−0.87	−0.84	−0.79
L	8	−4	−3	25.71	−0.96	−0.60	−0.75	−0.65
L	8	−4	3	25.71	−0.61	−0.60	−0.75	−0.65
L	12	−6	0	0.37	0.08	0.16	0.16	0.25
L	10	−5	−1	2.77	−0.26	−0.27	−0.25	−0.31
L	8	0	1	28.72	−0.03	−0.24	−0.19	0.12
L	8	0	0	12.43	0.02	−0.20	−0.10	−0.10
L	8	−1	−1	14.21	−0.89	−0.85	−0.56	−0.25
L	8	−1	1	10.19	−0.45	−0.35	−0.30	−0.37
L	8	−4	0	24.35	−0.16	−0.11	−0.25	−0.33
L	8	−5	3	25.31	−0.28	−0.22	0.02	0.51
L	8	−6	0	7.40	0.34	0.41	0.46	0.42
L	8	4	0	0.43	−2.00	−2.00	−1.95	−1.87
L	8	−4	2	37.11	−1.02	−0.88	−0.84	−0.79
C	7	−8	1	14.15	0.76	0.77	0.75	0.58
L	7	−8	1	14.13	0.89	0.77	0.76	0.58
L	6	−8	2	34.34	1.87	1.87	1.60	1.09
L	0	6	0	23.04	0.17	0.26	0.29	0.37

a priori hypotheses. In this study, atomic displacements induced by the field have been determined. When the electric field is applied along the [100] direction, deformations and reorientations of SiO_4 tetrahedra are induced while the Si-O distances are kept constant. The field induces angular variations of both intratetrahedral angles and bridging angles so that the rigid tetrahedra model proposed by Davasambuu et al. [7] is not confirmed. However, discrepancies on relative scattering variations induced by the field for some Bragg reflections also measured in [7] have been observed. Their origin is not clearly understood.

The structural model proposed in this study is consistent with the small values of the piezoelectric coefficients but further insight should be gained with the analysis of the field induced electron density polarisation of the Si-O bonds. We have undertaken measurements of Bragg intensity variations sensitive to the valence electron density (i.e. low order reflections) to clarify this aspect.

At last, analyses should also be carried out for other directions of the electric fields. However, in these cases, the resulting symmetry will be P1 with a larger number of parameters to be determined. In practical terms this means that the experiment will require a much longer time.

We are especially grateful to O. Cambon ande J. Haines (Université de Montpellier) for giving us a large single crystal of α quartz and for many discussions concerning the importance of this work, D. Yogev-Einot for the continous symmetry calculations. Many thanks to H. Graafsma and U. Pietsch for many fruitful discussions concerning the general lay out of our instrument and the delicate points in the data collection. We appreciate the help which we received from the company *Cristal Laser* for preparing the samples and B. Capelle (Université Paris VI) for verifying the crystal quality. We also acknowledge the continued support from LURE giving us very good working conditions throughout these past years.

Appendix A

Table 8 reports the squared structure factors, observed and calculated field induced variations for the three structural models. In the refinements a standard error of 0.1% on the relative intensity variations was used for all reflections. This error, superior to the counting statistics, is based on the stability and reproducibility of the experiment when repeating the measurement of the same reflection periodically. Reflections with $\sin\theta/\lambda < 0.7$ Å^{-1} (i.e. 8 reflections) and $\left|\eta_+^{obs} - \eta_+^{calc}\right| > 2\%$ (i.e. 4 reflections) are omitted in Table 8.

References

1. E. Philippot, D. Palmier, M. Pintard, A. Goiffon, J. Sol. State Chem. **123**, 1 (1996)
2. J. Haines, O. Cambon, Z. Kristallogr. **219**, 314 (2004)
3. A. Meissner, Zeitschrift Techn. Physik. **2**, 74 (1927)
4. R.F. Stewart, M.A. Whitehead, G. Donnay, Am. Min. **65**, 324 (1980)
5. U. Pietsch, J. Stahn, J. Davaasambuu, A. Pucher, J. Phys. Chem. Solids **62**, 2129 (2001)
6. J. Davaasambuu, Ph.D. thesis, University Potsdam, Germany (2003)
7. J. Davaasambuu, A. Pucher, V. Kochin, U. Pietsch, Europhys. Lett. **62**, 834 (2003)
8. S.C. Abrahams, Acta Cryst. A **50**, 658 (1994)
9. R. Puget, L. Godefroy, J. Appl. Cryst. A **46**, 297 (1975)
10. R. Guillot, P. Alle, P. Fertey, N.K. Hansen, E. Elkaim, J. Appl. Cryst. **35**, 360 (2002)
11. A.S. Bhalla, D. Bose, N.E.W. White, L.E. Cross, Phys. State. Sol. A **7**, 335 (1971)
12. G.R. Barsch, Acta Cryst. A **32**, 575 (1976)
13. N.K. Hansen, Computer programs of the Laboratory of Crystallography, Université Henri Poincaré
14. Y. Le Page, G. Donnay, Acta. Cryst. B **32**, 2456 (1976)
15. Landolt-Börnstein, *New series, supplementary III/18*, edited by K.H. Hellwege, A.M. Hellwege (Springer-Verlag, Berlin, 1984)
16. R.Guillot, Ph.D. thesis, Université Henri Poincaré – Nancy I, France (2002)
17. H. Zabrodsky, S. Peelg, D. Avnir, J. Am. Chem. Soc. **114**, 7843 (1992)
18. H. Zabrodsky, S. Peelg, D. Avnir, J. Am. Chem. Soc. **115**, 8278 (1993)
19. D. Yogev-Einot, D. Avnir, Chem. Mater. **15**, 464 (2003)
20. D. Yogev-Einot, D. Avnir, Acta Cryst. B **60**, 163 (2004)
21. L. Levien, C.T. Prewitt, J. Weidner, Am. Mineral. **65**, 920 (1980)
22. J. Glinnemann, H.E. King, H. Schulz, Th. Hahn, S.J. La Placa, F. Dacol, Z. Kristallogr. **198**, 177 (1992)